PHYSICAL REVIEW A **92**, 022508 (2015)

QED derivation of the Stark shift and line broadening induced by blackbody radiation

D. Solovyev,[1,*] L. Labzowsky,[1,2] and G. Plunien[3]

[1]*V. A. Fock Institute of Physics, St. Petersburg State University, Petrodvorets, Ulianovskaya 1, 198504, St. Petersburg, Russia*

[2]*Petersburg Nuclear Physics Institute, 188300, Gatchina, St. Petersburg, Russia*

[3]*Institut für Theoretische Physik, Technische Universität Dresden, Mommsenstrasse 13, D-01062 Dresden, Germany*

(Received 14 July 2015; published 20 August 2015)

The rigorous quantum electrodynamic approach is applied for the derivation of the Stark shift of the atomic energy levels induced by blackbody radiation (BBR) within the framework of perturbation theory. The temperature-dependent one-loop self-energy (SE) correction of bound atomic electron states accounting for the number of photons represented by the Planckian frequency-distribution function is examined. According to this approach, the energy shift arises as the real part of self-energy correction while the imaginary part describes the BBR-induced depopulation rate for a given atomic state. Moreover, regularization of the divergent energy denominators arising in the SE correction leads to an additional correction to the level width that has not been considered before and can be explained by the mixing effect of atomic levels in the presence of the BBR-induced mean electric field.

DOI: 10.1103/PhysRevA.92.022508 PACS number(s): 32.10.−f, 32.30.−r, 32.60.+i, 95.30.Dr

I. INTRODUCTION

The influence of blackbody radiation (BBR) on the atom is the one of the important topics in the modern atomic physics. Particular interests to such kind of investigations arise in view of the essential progress in the theoretical and experimental research of atomic clocks and determination of frequency standards. For the comprehensive theoretical description of the frequency standard, the analysis of the BBR influence on an atom is required [1,2]. In [1,2] it was demonstrated that the interaction with the BBR produces the efficient redistribution of population among closely lying levels. Moreover, the blackbody radiation at room temperature generates the so-called alternative current (ac) Stark shifts of atomic levels. The calculations of the dynamic Stark shifts and depopulation rates of Rydberg energy levels induced by blackbody radiation were widely discussed in literature [3–11].

According to [2], BBR efficiently redistributes population among Rydberg states, shortens the atomic lifetimes, and causes line broadening. The effective decay rate is given by

$$\Gamma_{\rm eff} = \Gamma_{\rm nt} + \Gamma_{\rm BBR}, \tag{1}$$

where $\Gamma_{\rm nt}$ represents the natural width of level and $\Gamma_{\rm BBR}$ is the BBR-induced width. There are two ways for the evaluation of $\Gamma_{\rm nt}$: (a) calculation of the sum of all the probabilities for transitions to lower-lying states and (b) evaluation of the imaginary part of the one-loop self-energy (SE) corrections. The first approach can be pursued within both quantum mechanics (QM) and relativistic quantum electrodynamics (QED). However, the rigorous evaluation of the imaginary part of SE [case b)] can be performed within the frameworks of the QED only. The derivation of the BBR-induced width $\Gamma_{\rm BB}$ for Rydberg levels on the base of QM approach was presented in [2] and final result (dipole approximation) can be given in SI units in the form

$$\Gamma_a^{\rm BBR} = \sum_b \Gamma_{a\to b}^{\rm BBR} = \frac{4e^2}{3\hbar c^3} \sum_{i,\,b} |\langle a|r_i|b\rangle|^2 \frac{\omega_{ab}^3}{e^{\frac{\hbar\omega_{ab}}{k_B T}} - 1}, \tag{2}$$

where e is the electron charge, $\hbar$ is the reduced Planck's constant, and c is the speed of light. Boltzman's constant is denoted by k_B, T represents the temperature of the blackbody radiation, r_i is the component of the spatial position vector of an atomic electron, and a, b correspond to all the quantum numbers of atomic levels a and b, respectively. The last factor in Eq. (2) can be attributed to the temperature-dependent statistical average $\langle E^2(\omega)\rangle_\beta \sim \omega^3 \langle \hat{n}(\omega)\rangle_\beta = \omega^3 n_\beta(\omega)$ with $\beta = 1/K_B T$ associated with the fluctuation of electric field mode $E(\omega)$ with frequency ω contributing to the mean energy of the radiation field; it may also be viewed as temporal average

$$\langle E^2(\omega)\rangle_t = \frac{8\alpha^3}{\pi} \frac{\omega^3}{e^{\frac{\omega}{k_B T}} - 1} = \frac{8\alpha^3}{\pi}\, \omega^3\, n_\beta(\omega)\,, \tag{3}$$

where α is the fine-structure constant and angular brackets with the index t $\langle\cdots\rangle_t$ correspond to the averaging over time [7]. $n_\beta(\omega)$ denotes the mean occupation number of the field mode. Here, atomic units ($\hbar = m_e = c = 1$) are used (m_e is the mass of the electron).

According to [1] these fields induce temperature-dependent shifts of transition frequencies in atoms and molecules through the alternative current (ac) Stark effect which can be estimated via the mean-squared field

$$\langle E^2\rangle_t = \frac{1}{2}\int_0^\infty \langle E^2(\omega)\rangle_t d\omega = \frac{4\pi^3}{15}\alpha^3 (k_B T)^4$$
$$= (8.319\ \text{V/cm})^2 [\text{T(K)}/300]^4. \tag{4}$$

In this paper, we will provide explicit derivations of the finite-temperature effects connected with the BBR influence on atomic levels on the basis of the rigorous bound-state QED approach. For this purpose we apply the finite-temperature QED describtion involving free electrons and photons developed earlier by Donoghue and Holstein [12] to atoms interacting with a photon heat bath. Consequently, we recover the known expressions for the BBR-induced ac Stark shift and for the level broadening connected with the atomic level depopulation. Moreover, we find another BBR contribution to the level broadening, namely, the broadening caused by the opposite parity level mixing in the mean BBR electric

*solovyev.d@gmail.com

field. This contribution appears to be as important as the depopulation broadening. This effect can be traced also phenomenologically within the framework of QM, however, only the QED derivation clarifies the difference between depopulation and mixing broadening effects.

Although major phenomenological interest in the BBR investigation in laboratory studies is governed by atomic clocks studies on heavy neutral atoms and ions, our numerical results reported in this paper will focus exclusively on the hydrogen atom. The hydrogen atom was chosen for two reasons: First, this atom is the most simple and suitable object for QED studies; the extension of the calculations to many-electron atoms seems to be straightforward. Second, our results demonstrate the importance of the Stark-mixing contribution to the level broadening at temperatures of about 3000 K corresponding to the cosmological recombination epoch of the universe. So, this effect should be taken into account also in astrophysics.

Our paper is organized as follows. In Sec. II, we remind the standard QED expression for one-loop electron self-energy at zero temperature in the form suitable, which also allows for generalization to finite-temperature QED including further application to BBR. In Sec. III, the QED description of atomic system interacting with a heat bath is introduced mainly on the basis of the photon propagator at finite temperature. In Sec. IV, we evaluate the BBR-induced shift and broadening of atomic levels via the QED approach. Section V contains the derivation of the level broadening via Stark level mixing, Sec. VI contains the numerical results, and Sec. VII is devoted to the conclusions.

II. ONE-LOOP ELECTRON SELF-ENERGY CORRECTION AT ZERO TEMPERATURE

Within the framework of bound-state QED at zero temperature, the one-loop electron self-energy correction for an atomic electron corresponds to the Feynman graph Fig. 1, where the atomic electron interacts with the photon vacuum (virtual photons only). A generic nondiagonal second-order S-matrix element in the Furry picture for a bound atomic electron looks like

$$\langle a'|\hat{S}^{(2)}|a\rangle = e^2 \int d^4x_1 d^4x_2 \bar{\psi}_{a'}(x_1)\gamma^{\mu_1} S(x_1,x_2) \times \gamma^{\mu_2}\psi_a(x_2) D_{\mu_1\mu_2}(x_2,x_1), \quad (5)$$

where integration is performed over spacetime variables x_1, x_2 which denote abbreviatively the spatial position vector $\vec{r}$ and the time variable t. Here, we employ relativistic units $\hbar = c = 1$. The Dirac matrices are denoted as γ_{μ_i}, where μ_i takes the values $\mu_i = (1,2,3,4)$, $\psi_a(x) = \psi_a(\vec{r})e^{-iE_a t}$ is the one-electron Dirac wave function, $\bar{\psi}_a$ is the Dirac conjugated wave function. The standard (zero-temperature) electron propagator defined as vacuum-expectation value of the time-ordered product can be represented in terms of an eigenmode decomposition with respect to one-electron eigenstates:

$$S(x_1,x_2) = -i\langle 0|T[\psi(x_1)\bar{\psi}(x_2)]|0\rangle$$

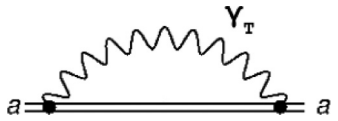

FIG. 1. The thermal one-loop self-energy correction for the energy of an atomic electron in a level a. The double solid line denotes the electron states and electron propagator in the external potential of the nucleus (Furry picture). The internal wavy line denotes the virtual photon (ordinary photon propagator), while the photon line together with the index γ_T implies the inclusion of BBR photons distributed with the function $n_\beta(\omega)$ (thermal photon propagator).

$$= \frac{i}{2\pi}\int_{-\infty}^{\infty} d\omega\, e^{-i\omega(t_1-t_2)} \sum_n \frac{\psi_n(\vec{r}_1)\bar{\psi}_n(\vec{r}_2)}{\omega - E_n(1-i0)}, \quad (6)$$

where summation runs over the entire Dirac spectrum. Finally, the standard (zero-temperature) photon propagator $D^0_{\mu_1\mu_2}(x_2,x_1)$ in Feynman gauge reads as

$$D^0_{\mu_1\mu_2}(x_2,x_1) = -i\langle 0|T\left[A_{\mu_1}(x_1)A_{\mu_2}(x_2)\right]|0\rangle = \frac{i}{2\pi}\int_{-\infty}^{\infty} d\Omega\, I_{\mu_1\mu_2}(|\Omega|,r_{12})e^{-i\Omega(t_2-t_1)} \quad (7)$$

together with the notation

$$I_{\mu_1\mu_2}(\Omega,r_{12}) = \frac{g_{\mu_1\mu_2}}{r_{12}} e^{i\Omega r_{12}}, \quad (8)$$

where $r_{12} = |\vec{r}_1 - \vec{r}_2|$ and $g_{\mu_1\mu_2}$ is the metric tensor (we employ the pseudo-Euclidean metric). The energy correction ΔE_a for "irreducible" Feynman graph can be obtained via the relation [13,14]

$$\langle a'|\hat{S}^{(2)}|a\rangle = -2\pi i\langle a'|U|a\rangle\delta(E_{a'} - E_a), \quad (9)$$

$$\Delta E_a = \langle a|U|a\rangle. \quad (10)$$

Performing the integration over time and ω variables leads to

$$\Delta E_a = \frac{e^2}{2\pi i}\sum_n \left[\frac{1-\vec{\alpha}_1\vec{\alpha}_2}{r_{12}} I_{na}(r_{12})\right]_{anna}, \quad (11)$$

where

$$I_{na}(r_{12}) = \int_{-\infty}^{\infty} \frac{e^{i|\omega|r_{12}}d\omega}{E_n(1-i0) - E_a + \omega}, \quad (12)$$

$\vec{\alpha}$ is the Dirac matrix, and

$$[\hat{A}(12)]_{abcd} \equiv \langle a(1)b(2)|\hat{A}|c(1)d(2)\rangle. \quad (13)$$

Correction ΔE_a can be presented in a standard form

$$\Delta E_a = L_a^{(\mathrm{SE})} - \frac{i}{2}\Gamma_a. \quad (14)$$

Here, $L_a^{(\mathrm{SE})}$ denotes the lowest-order electron self-energy contribution to the Lamb shift and Γ_a denotes the lowest-order radiative width. The other lowest-order radiative correction giving rise to the energy shift is the vacuum polarization correction which does not contribute however to Γ_a. The description of renormalization of the divergent real part of ΔE_a within QED theory lies beyond of our interests in this paper.

Consideration of the lowest-order radiative corrections (real and imaginary parts) allows for the development of the line profile approach (LPA) [14]. Within this approach, the regularization of the singularities in the amplitude of photon scattering process on atomic electron naturally arises. In the case of resonant photon scattering process the account for the sequence of SE (one loop, two loop, etc.) corrections leads to geometric progression and the corresponding regularization of the divergent energy denominators. The detailed analysis of the imaginary part of the higher-order SE corrections can be found in [15].

III. PHOTON PROPAGATOR AT FINITE TEMPERATURE

Up to now, we have considered only the radiative corrections within standard (zero-temperature) QED theory, i.e., with one virtual photon [see Eq. (7)]. Under more realistic conditions, however, the photon field is not in its vacuum state. Instead, the electrons bound in an atom (system) interact with thermal photons considered as heat bath (environment). Such a scenario is well suited for the application of thermal-equilibrium quantum field theory. Accordingly, when aiming at a proper description of QED corrections, the usual ($T = 0$) photon propagator $D^0_{\mu_1\mu_2}$ should be replaced by the ensemble-averaged time-ordered product

$$\begin{aligned} i\,D_{\mu_1\mu_2}(x_1,x_2|\beta) &= \big\langle \mathrm{T}\big[A_{\mu_1}(x_1)A_{\mu_2}(x_2)\big]\big\rangle_\beta \\ &= \mathrm{Tr}\big(\rho\big\{\mathrm{T}\big[A_{\mu_1}(x_1)A_{\mu_2}(x_2)\big]\big\}\big) \\ &= i\,D^0_{\mu_1\mu_2}(x_1,x_2) + i\,D^\beta_{\mu_1\mu_2}(x_1,x_2)\,, \end{aligned} \tag{15}$$

where ρ denotes (in zeroth approximation) the statistical operator for noninteracting photons, electrons, and positrons. The trace Tr runs over all (multiparticle) Fock states. This ansatz is legitimate if no free electrons or positrons are present as well as for temperatures $k_B T \ll m_e c^2$. According to Wick's theorem, the time-ordered product of the photon-field operators can be decomposed as sum of a contraction (vacuum-expectation value of the T product) plus normal-ordered ($:\cdots:$) product

$$\begin{aligned} \big\langle \mathrm{T}\big[A_{\mu_1}(x_1)A_{\mu_2}(x_2)\big]\big\rangle_\beta &= \langle 0|\mathrm{T}\big[A_{\mu_1}(x_1)A_{\mu_2}(x_2)\big]|0\rangle \\ &\quad + \big\langle :A_{\mu_1}(x_1)A_{\mu_2}(x_2):\big\rangle_\beta\,. \end{aligned} \tag{16}$$

Thus, the finite-temperature photon propagator (15) appears as sum of the zero-temperature part $D^0_{\mu_1\mu_2}$ plus the thermal part $D^\beta_{\mu_1\mu_2}$ involving Planck's frequency distribution for the photons of the heat bath. In this section, we will account for this and, in particular, we are interested in the influence of blackbody radiation on the atomic characteristics. Then, the thermal averaged number of photons $n_\beta(\omega)$ in the frequency mode ω as given by Planck's distribution function should be employed:

$$\begin{aligned} n_\beta(\omega) &= \frac{1}{e^{\frac{\omega}{k_B T}} - 1}\,, \quad \omega > 0 \\ n_\beta(\omega) &= 0, \quad \omega < 0 \end{aligned} \tag{17}$$

where $\beta = (k_B T)^{-1}$ and T is the temperature in Kelvin.

To reveal the effects arising via the inclusion of distribution function (17), we refer to the finite-temperatures QED approach developed by Donoghue and Holstein [12]. Within the approach of Donoghue and Holstein (DH), a free-electron gas (no external field) interacts with a photon gas is considered as being in thermal equilibrium and described by a grand canonical statistical operator, which modifies both the electron and the photon propagator. Since our task is to consider the influence of the BBR on atomic levels, we retain the electron propagator in the form (6) and will treat the influence of the BBR within QED perturbation theory involving the the thermal photon propagator.

According to [12], the thermal photon propagator in the momentum space reads as

$$D^{\mathrm{DH}}_{\mu\nu}(k) = -g^{\mu\nu}\left[\frac{i}{k^2 + i\epsilon} + 2\pi\,\delta(k^2) n_\beta(\omega)\right], \tag{18}$$

where k is the four-dimensional momentum, $k^2 = \vec{k}^2 - \omega^2$, and $n_\beta(\omega_k)$ is defined by Eq. (17). In the coordinate space we obtain

$$\begin{aligned} D^{\mathrm{DH}}_{\mu\nu}(x_1, x_2) &= -4\pi i g_{\mu\nu} \int \frac{d^4k}{(2\pi)^4} e^{ik(x_1 - x_2)} \\ &\quad \times \left[\frac{1}{k^2 + i\epsilon} - 2\pi i\,\delta(k^2) n_\beta(\omega)\right]. \end{aligned} \tag{19}$$

The expression in Eq. (19) can be evaluated in the standard way, i.e., the z axis in $\vec{k}$ space can be chosen along the direction of vector $\vec{r}$. After the integration over angles we find (denoting $|\vec{k}| \equiv \kappa$)

$$\begin{aligned} D^{\mathrm{DH}}_{\mu\nu}(x_1, x_2) &= -\frac{4\pi i g_{\mu\nu}}{(2\pi)^4} \int d\vec{k}\, d\omega \left[\frac{e^{i\vec{k}(\vec{r}_1 - \vec{r}_2) - i\omega(t_1 - t_2)}}{k^2 + i\epsilon} - 2\pi i e^{i\vec{k}(\vec{r}_1 - \vec{r}_2) - i\omega(t_1 - t_2)} \delta(k^2) n_\beta(\omega)\right] \\ &= -\frac{(4\pi)^2 i g_{\mu\nu}}{(2\pi)^4} \int_{-\infty}^{+\infty} d\omega \int_0^{+\infty} d\kappa \frac{\kappa}{r_{12}} \sin\kappa r_{12} e^{-i\omega(t_1 - t_2)} \left[\frac{1}{\kappa^2 - \omega^2 + i\epsilon} - 2\pi i\,\delta(\kappa^2 - \omega^2) n_\beta(\omega)\right] \\ &= D^0_{\mu\nu}(x_1, x_2) + D^\beta_{\mu\nu}(x_1, x_2). \end{aligned} \tag{20}$$

Then, integration in complex plane κ with account for poles $\kappa_{1,2} = \pm\sqrt{\omega^2 + i\epsilon} \approx \pm\omega \pm i\epsilon$ for the first term in Eq. (20) leads to the standard expression

$$D^0_{\mu\nu}(x_1, x_2) = \frac{g_{\mu\nu}}{2\pi i r_{12}} \int_{-\infty}^{+\infty} d\omega\, e^{i|\omega| r_{12} - i\omega(t_1 - t_2)}. \tag{21}$$

The second term in Eq. (20) can be evaluated with the relation

$$\delta(x^2 - a^2) = \frac{1}{2a}[\delta(x - a) + \delta(x + a)]. \tag{22}$$

This yields

$$D^{\beta}_{\mu\nu}(x_1, x_2) = -\frac{g_{\mu\nu}}{\pi r_{12}} \int_{-\infty}^{+\infty} d\omega\, n_\beta(|\omega|) \sin|\omega| r_{12} e^{-i\omega(t_1 - t_2)}. \tag{23}$$

Finally,

$$D^{\mathrm{DH}}_{\mu\nu}(x_1, x_2) = \frac{g_{\mu\nu}}{2\pi i r_{12}} \int_{-\infty}^{+\infty} d\omega\, e^{i|\omega| r_{12} - i\omega(t_1 - t_2)} - \frac{g_{\mu\nu}}{\pi r_{12}} \int_{-\infty}^{+\infty} d\omega\, n_\beta(|\omega|) \sin|\omega| r_{12} e^{-i\omega(t_1 - t_2)}. \tag{24}$$

We should note that in the calculations of the energy correction ΔE_a with $D^{\beta}_{\mu\nu}$ to first order in α, no ultraviolet divergence arises because the function $n_\beta(\omega)$ provides a natural cutoff for the ultraviolet divergence [12] (see also [16] and references therein).

IV. EVALUATION OF ONE-LOOP ELECTRON SELF-ENERGY CORRECTION IN PRESENCE OF BBR

A. Real part of the one-loop self-energy correction

We consider now the real part of the one-loop electron self-energy correction with the inclusion of the photon number $n_\beta(\omega)$. For this purpose, we replace the photon propagator $D^0_{\mu\nu}$ in Eq. (5) by $D^{\mathrm{DH}}_{\mu\nu}$. Then, the energy shift is

$$\Delta E^{\beta}_a = \frac{e^2}{\pi} \sum_n \left[\frac{1 - \vec{\alpha}_1 \vec{\alpha}_2}{r_{12}} I^{\beta}_{na}(r_{12}) \right]_{anna}, \tag{25}$$

where

$$I^{\beta}_{na}(r_{12}) = \int_{-\infty}^{+\infty} d\omega\, n_\beta(|\omega|) \frac{\sin|\omega| r_{12}}{E_n(1 - i0) - E_a + \omega}. \tag{26}$$

Explicit insertion of the sign of modulus in Eq. (26) yields

$$I^{\beta}_{na}(r_{12}) = \int_0^{+\infty} d\omega\, n_\beta(\omega) \frac{\sin\omega r_{12}}{E_n(1 - i0) - E_a + \omega} + \int_{-\infty}^{0} d\omega\, n_\beta(-\omega) \frac{-\sin\omega r_{12}}{E_n(1 - i0) - E_a + \omega}. \tag{27}$$

Change of the variable $\omega \to -\omega$ in the second term in Eq. (27) gives

$$I^{\beta}_{na}(r_{12}) = \int_0^{+\infty} d\omega\, n_\beta(\omega) \sin\omega r_{12} \left[\frac{1}{E_n(1 - i0) - E_a + \omega} + \frac{1}{E_n(1 - i0) - E_a - \omega} \right]. \tag{28}$$

Further, we can use the relation

$$\lim_{\epsilon \to 0} \frac{1}{x \pm i\epsilon} = \mathrm{P.\,V.}\left(\frac{1}{x}\right) \mp i\pi\delta(x), \tag{29}$$

where P. V. means the principal value. Then, expression (28) can be transformed to

$$I^{\beta}_{na}(r_{12}) = \mathrm{P.\,V.} \int_0^{+\infty} d\omega\, n_\beta(\omega) \sin\omega r_{12} \frac{2\omega_{na}}{\omega^2_{na} - \omega^2} + i\pi \int_0^{+\infty} d\omega\, n_\beta(\omega) \sin\omega r_{12} [\delta(\omega_{na} - \omega) + \delta(\omega_{na} + \omega)], \tag{30}$$

where the notation $\omega_{na} = E_n - E_a$ was introduced.

Insertion of Eq. (30) into Eq. (25) leads to an expression which consists of the real part [first term in Eq. (30)] and the imaginary part arising via the second term in Eq. (30). The expression for the real part of the energy shift simplifies significantly in the nonrelativistic limit. The function $n_\beta(\omega)$ is localized between zero and ionization potential I at any reasonable temperatures (up to $\approx$10 000 K) for the neutral hydrogen atom and low-Z hydrogenlike ions. The value of I equals to $\frac{1}{2} m_e (\alpha Z)^2$ r.u. where Z is the charge of the nucleus in the units of e. In the nonrelativistic limit we can use the dipole approximation, when $\omega \sim m_e(\alpha Z)^2$ r.u., $r_{12} \sim 1/(m_e \alpha Z)$ r.u., and $\omega r \sim (\alpha Z) \ll 1$. Expanding the $\sin\omega r_{12}$ into the Taylor series we need to keep the two leading terms. Then, the real part of Eq. (25) can be written as

$$\begin{aligned} \mathrm{Re}\Delta E^{\beta}_a &= \frac{e^2}{\pi} \sum_n \left\{ \mathrm{P.\,V.} \int_0^{+\infty} d\omega\, n_\beta(\omega) \frac{1 - \vec{\alpha}_1 \vec{\alpha}_2}{r_{12}} \left[\omega r_{12} - \frac{1}{6} (\omega r_{12})^3 \right] \frac{2\omega_{na}}{\omega^2_{na} - \omega^2} \right\}_{anna} \\ &= \frac{e^2}{\pi} \sum_n \left[\mathrm{P.\,V.} \int_0^{+\infty} d\omega\, n_\beta(\omega) \left(-\omega \vec{\alpha}_1 \vec{\alpha}_2 - \frac{1}{6} \omega^3 r^2_{12} \right) \frac{2\omega_{na}}{\omega^2_{na} - \omega^2} \right]_{anna}. \end{aligned} \tag{31}$$

The term containing ωr_{12} in Eq. (31) gives the zero due to the orthogonality of the wave functions. To complete the evaluation of Eq. (31) in the nonrelativistic limit, we suggest that the main contribution to the integral in Eq. (31) comes from the region $\omega \approx \omega_{na}$. Then, using relations $(\vec{\alpha})_{ab} \simeq (\vec{p})_{ab} = i\omega_{ab}(\vec{r})_{ab}, r^2_{12} = r^2_1 + r^2_2 - 2(\vec{r}_1 \vec{r}_2)$, we find

$$\mathrm{Re}\Delta E^{\beta}_a = \frac{4e^2}{3\pi} \sum_n \int_0^{\infty} n_\beta(\omega) \omega^3 |\langle a|\vec{r}|n\rangle|^2 \frac{\omega_{an}}{\omega^2_{na} - \omega^2} d\omega. \tag{32}$$

The integral over ω in Eq. (32) should be understood if necessary in a sense of principal value.

Note that Eq. (31) contains the sum over intermediate states from the negative spectrum. The contribution of negative energy part of spectrum can be evaluated in the nonrelativistic limit as well. For the two-photon transition probabilities, it was done in [17]. However, the contribution of the negative energy part represents a small correction to Eq. (32). Thus, the sum in Eq. (32) runs over positive energies (discrete and continuum) only. Inserting Eq. (17) in Eq. (32), we find that the result for the real part of the energy shift $\mathrm{Re}\Delta E_a^\beta$ coincides precisely with the definition of ac Stark shift given in [2].

B. Imaginary part of one-loop electron self-energy correction

Let us now turn to the imaginary part of one-loop self-energy correction (25) with account for the photon distribution $n_\beta(\omega)$. As before, we use the expression (30) for $I_{na}^\beta(r_{12})$. Then, the imaginary part of energy shift (25) looks like

$$\mathrm{Im}\Delta E_a^\beta = e^2 \sum_n \left\{ \frac{1-\vec{\alpha}_1\vec{\alpha}_2}{r_{12}} \int_0^{+\infty} d\omega\, n_\beta(\omega) \sin\omega r_{12} \times [\delta(\omega_{na}-\omega)+\delta(\omega_{na}+\omega)] \right\}_{anna}. \quad (33)$$

Integration over ω leads to

$$\mathrm{Im}\Delta E_a^\beta = e^2 \sum_n \left[\frac{1-\vec{\alpha}_1\vec{\alpha}_2}{r_{12}} n_\beta(\omega_{na}) \sin\omega_{na} r_{12} \right]_{anna} - e^2 \sum_n \left[\frac{1-\vec{\alpha}_1\vec{\alpha}_2}{r_{12}} n_\beta(-\omega_{na}) \sin\omega_{na} r_{12} \right]_{anna}. \quad (34)$$

Using the properties of the function $n_\beta(\omega)$, we can conclude that the first term in Eq. (34) is nonzero for $E_n > E_a$ and, in contrast, the second term is nonzero for $E_n < E_a$. Therefore, we can further write

$$\mathrm{Im}\Delta E_a^\beta = e^2 \sum_{E_n>E_a} \left[\frac{1-\vec{\alpha}_1\vec{\alpha}_2}{r_{12}} n_\beta(\omega_{na}) \sin\omega_{na} r_{12} \right]_{anna} + e^2 \sum_{E_n<E_a} \left[\frac{1-\vec{\alpha}_1\vec{\alpha}_2}{r_{12}} n_\beta(\omega_{an}) \sin\omega_{an} r_{12} \right]_{anna}. \quad (35)$$

Employing again the approximations made in the previous section, we obtain in the nonrelativistic limit

$$\mathrm{Im}\Delta E_a^\beta = -\frac{2}{3} e^2 \sum_n |\langle a|\vec{r}|n\rangle|^2 n_\beta(|\omega_{an}|)\omega_{an}^3. \quad (36)$$

In Eq. (36), the sign of terms in Eq. (34) is taken into account automatically with the modulus notation. Using the definition of Γ_a in Eq. (14) we arrive at

$$\Gamma_a^\beta = \frac{4}{3} e^2 \sum_n |\langle a|\vec{r}|n\rangle|^2 n_\beta(|\omega_{an}|)\omega_{an}^3. \quad (37)$$

Thus, substitution of Eq. (17) into the expression (37) results in the BBR-induced level width as defined in [2].

V. QED REGULARIZATION AND STARK-MIXING BROADENING

In the previous section we have considered the one-loop thermal electron self-energy correction with account for the distribution function over the photons $n_\beta(\omega)$ (see Fig. 1). The QED evaluation confirms the known results, i.e., the real part of the correction (25) gives the ac Stark shift and the imaginary part corresponds to the BBR-induced level width. However, these results were obtained without the account for the ordinary Lamb shift for atomic states. In this section, we consider especially the case when the energy denominator in Eq. (28) becomes singular, i.e., when $\omega = E_n - E_a$. The QED regularization procedure consists in an inclusion of the ordinary one-loop self-energy corrections into the corresponding S-matrix element, thermal loop (25) in our case. In this case, the Feynman diagrams depicted in Fig. 2 should be evaluated [14].

The energy shift corresponding to the Feynman graph Fig. 2(b) is defined by

$$\Delta E_a^\beta = \frac{e^4}{2\pi^2 i} \sum_{n\,m\,k} \int_{-\infty}^{+\infty} d\omega_1 \int_{-\infty}^{\infty} d\omega_2 \frac{\langle\psi_a(\vec{r}_1)\psi_m(\vec{r}_4)|\frac{1-\vec{\alpha}_1\vec{\alpha}_4}{r_{14}} n_\beta(|\omega_1|)\sin(|\omega_1|r_{14})|\psi_n(\vec{r}_1)\psi_a(\vec{r}_4)\rangle}{[E_n(1-i0)-E_a+\omega_1][E_m(1-i0)-E_a+\omega_1]} \times \frac{\langle\psi_n(\vec{r}_2)\psi_k(\vec{r}_3)|\frac{1-\vec{\alpha}_2\vec{\alpha}_3}{r_{23}} e^{i|\omega_2|r_{23}}|\psi_k(\vec{r}_2)\psi_m(\vec{r}_3)\rangle}{E_k(1-i0)-E_a+\omega_1+\omega_2}, \quad (38)$$

where the first factor under the integral represents the thermal one-loop self-energy (SE) correction and the last factor is the ordinary ($T=0$) one-loop QED self-energy correction.

Introducing the notation for the matrix element of the ordinary self-energy operator [14] and for the matrix element which enters the expression for the thermal SE

$$[\widehat{\Sigma}(\xi)]_{u\,d} = -\frac{e^2}{2\pi i} \sum_k \int_{-\infty}^{\infty} d\omega_2 \frac{\langle\psi_u(\vec{r}_2)\psi_k(\vec{r}_3)|\frac{1-\vec{\alpha}_2\vec{\alpha}_3}{r_{23}} e^{i|\omega_2|r_{23}}|\psi_k(\vec{r}_2)\psi_d(\vec{r}_3)\rangle}{E_k(1-i0)+\omega_2-\xi},$$
$$[\widehat{\Sigma}^\beta(\xi)]_{a\,b\,c\,d} = \langle\psi_a(\vec{r}_1)\psi_b(\vec{r}_4)|\frac{1-\vec{\alpha}_1\vec{\alpha}_4}{r_{14}} n_\beta(|\omega_1|)\sin(|\xi|r_{14})|\psi_c(\vec{r}_1)\psi_d(\vec{r}_4)\rangle, \quad (39)$$

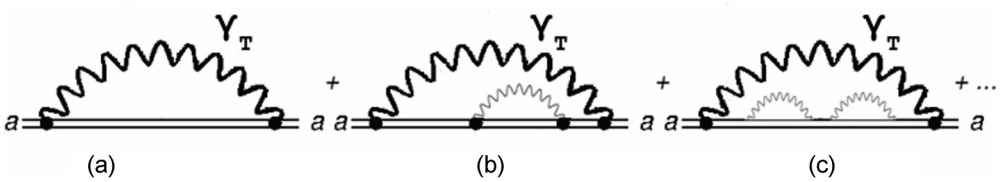

FIG. 2. Insertions of "ordinary" one-loop self-energy correction into the thermal one-loop self-energy correction leading to a "dressed" electron propagator [see graphs (a), (b), (c)]. The internal wavy line denotes the virtual photon (ordinary photon propagator), while the photon line together with the index γ_T corresponds to the thermal photon loop (including the BBR photons).

the energy shift corresponding to the Feynman graph Fig. 2(b) can be written in the form

$$\begin{aligned}\Delta^{(1)}E_a^\beta &= \frac{e^2}{\pi}\sum_{n\,m}\int_{-\infty}^{+\infty} d\omega_1 \frac{\langle\psi_a(\vec{r}_1)\psi_m(\vec{r}_4)|\frac{1-\vec{\alpha}_1\vec{\alpha}_4}{r_{14}} n_\beta(|\omega_1|)\sin(|\omega_1|r_{14})|\psi_n(\vec{r}_1)\psi_a(\vec{r}_4)\rangle[\widehat{\Sigma}(E_a-\omega_1)]_{n\,m}}{[E_n(1-i0)-E_a+\omega_1][E_m(1-i0)-E_a+\omega_1]}\\ &= \frac{e^2}{\pi}\sum_{n\,m}\int_{-\infty}^{+\infty} d\omega_1 \frac{[\widehat{\Sigma}^\beta(\omega_1)]_{a\,m\,n\,a}}{E_n(1-i0)-E_a+\omega_1}\frac{[\widehat{\Sigma}(E_a-\omega_1)]_{n\,m}}{E_m(1-i0)-E_a+\omega_1}.\end{aligned} \tag{40}$$

The sum of the self-energy corrections Figs. 2(a) and 2(b) is given by

$$\Delta E_a^\beta + \Delta^{(1)}E_a^\beta = \frac{e^2}{\pi}\sum_{n}\int_{-\infty}^{+\infty} d\omega_1 \frac{[\widehat{\Sigma}^\beta(\omega_1)]_{a\,n\,n\,a}}{E_n(1-i0)-E_a+\omega_1} + \frac{e^2}{\pi}\sum_{n\,m}\int_{-\infty}^{+\infty} d\omega_1 \frac{[\widehat{\Sigma}^\beta(\omega_1)]_{a\,m\,n\,a}}{E_n(1-i0)-E_a+\omega_1}\frac{[\widehat{\Sigma}(E_a-\omega_1)]_{n\,m}}{E_m(1-i0)-E_a+\omega_1}. \tag{41}$$

Within the resonance approximation [14] we restrict ourselves with one term $m=n$ only and thus write

$$\Delta E_a^\beta + \Delta^{(1)}E_a^\beta = \frac{e^2}{\pi}\sum_{n}\int_{-\infty}^{+\infty} d\omega_1 \frac{[\widehat{\Sigma}^\beta(\omega_1)]_{a\,n\,n\,a}}{E_n(1-i0)-E_a+\omega_1}\left\{1+\frac{[\widehat{\Sigma}(E_a-\omega_1)]_{n\,n}}{E_n(1-i0)-E_a+\omega_1}\right\}. \tag{42}$$

Repeating such insertions within the resonance approximation [the next term of this series is depicted in Fig. 2(c)], we arrive at the geometric progression that gives

$$\widetilde{\Delta E}_a^\beta = \frac{e^2}{\pi}\sum_{n}\int_{-\infty}^{+\infty} d\omega_1 \frac{[\widehat{\Sigma}^\beta(\omega_1)]_{a\,n\,n\,a}}{[E_n(1-i0)-E_a+\omega_1]\{1-\frac{[\widehat{\Sigma}(E_a-\omega_1)]_{n\,n}}{E_n(1-i0)-E_a+\omega_1}\}}. \tag{43}$$

Within the resonance approximation operator $\widehat{\Sigma}(E_a-\omega_1)$ can be expanded in a Taylor series around the value $E_a-\omega_1=E_n$. Employing the definition $[\widehat{\Sigma}(E_n)]_{n\,n}=L_n^{\rm SE}-\frac{i}{2}\Gamma_n$, the final expression is

$$\widetilde{\Delta E}_a^\beta = \frac{e^2}{\pi}\sum_{n}\int_{-\infty}^{+\infty} d\omega\, n_\beta(|\omega|)\frac{\langle a\,n|\frac{1-\vec{\alpha}_1\vec{\alpha}_2}{r_{12}}\sin(|\omega|r_{12})|n\,a\rangle}{E_n+\omega-E_a+L_n^{\rm SE}-\frac{i}{2}\Gamma_n}, \tag{44}$$

where $L_n^{\rm SE}$ is the Lamb shift and Γ_n is the natural level width of the nth level.

Apart from the self-energy correction, the vacuum-polarization insertions in the electron propagator to all orders should be also considered within the resonance approximation. Similarly, the resulting geometric progression of the vacuum-polarization corrections contributes to the real part of energy shift only and, thus, the total Lamb shift of nth state $L_n^{\rm SE}+L_n^{\rm VP}$ does arrive. With a somewhat more involved procedure, the self-energy and vacuum-polarization correction for the state a (wave-function corrections) can be taken into account. Finally, the sum of widths and difference of Lamb shifts for the states n and a can be inserted in the electron propagator [14].

Further evaluation of the expression (44) can be made as in the previous section. Accordingly, we arrive at the expression

$$\begin{aligned}\widetilde{\Delta E}_a^\beta = \frac{e^2}{\pi}\sum_{n}\int_{0}^{+\infty} d\omega\, n_\beta(\omega)\langle a\,n|\frac{1-\vec{\alpha}_1\vec{\alpha}_2}{r_{12}}\sin\omega r_{12}|n\,a\rangle\\ \times\left[\frac{1}{E_n-E_a+\omega+L_n^{\rm SE}+L_n^{\rm VP}-\frac{i}{2}\Gamma_n}+\frac{1}{E_n-E_a-\omega+L_n^{\rm SE}+L_n^{\rm VP}-\frac{i}{2}\Gamma_n}\right].\end{aligned} \tag{45}$$

Equation (45) differs from Eq. (28) by presence of the Lamb shift $L_n^{\rm SE}+L_n^{\rm VP}$ and the natural level width Γ_n. In contrast to evaluations made in the previous section, we do not need to use Eq. (29) anymore.

In the nonrelativistic limit we have

$$\widetilde{\Delta E}_a^{\beta} = -\frac{e^2}{\pi}\sum_n \int_0^{+\infty} d\omega\, n_\beta(\omega)\omega |\langle a|\vec{p}|n\rangle|^2 \left[\frac{1}{E_n - E_a + \omega + \Delta E_{na}^L - \frac{i}{2}\Gamma_{na}} + \frac{1}{E_n - E_a - \omega + \Delta E_{na}^L - \frac{i}{2}\Gamma_{na}}\right]$$
$$+ \frac{e^2}{3\pi}\sum_n \int_0^{+\infty} d\omega\, n_\beta(\omega)\omega^3 |\langle a|\vec{r}|n\rangle|^2 \left[\frac{1}{E_n - E_a + \omega + \Delta E_{na}^L - \frac{i}{2}\Gamma_{na}} + \frac{1}{E_n - E_a - \omega + \Delta E_{na}^L - \frac{i}{2}\Gamma_{na}}\right], \quad (46)$$

where $\vec{p}$ is the atomic electron momentum, $\Delta E_{na}^L = L_n^{\rm SE} + L_n^{\rm VP} - L_a^{\rm SE} - L_a^{\rm VP}$, and Γ_{na} represents the sum of level widths $\Gamma_{na} = \Gamma_n + \Gamma_a$.

As in the previous section, the total thermal shift consists of the real and imaginary parts. The real part represents again the ac Stark shift with the Lamb shift of the atomic levels taken into account. This part does not differ in any serious way from the results obtained earlier with the neglect of the Lamb shift. However, the imaginary part contains now two contributions. The "old" contribution is responsible for the depopulation of atomic levels by the BBR and does not differ from the results described in Sec. IV B. The "new" part describes a different physical effect: mixing of the atomic states by the mean electric field induced by the BBR. This effect can be of course traced in the frames of QM approach (see following) but the QED treatment makes it quite clear that the level mixing effect is different from the level depopulation effect. All these effects one-by-one will be considered in this section.

A. Real part: ac Stark contribution

To evaluate the real and imaginary parts of Eq. (46) separately, we rewrite the energy shift $\widetilde{\Delta E}_a^{\beta}$ in the form

$$\widetilde{\Delta E}_a^{\beta} = -\frac{e^2}{\pi}\sum_n |\langle a|\vec{r}|n\rangle|^2 \int_0^{\infty} d\omega\, n_\beta(\omega)\left(\omega\tilde{\omega}_{an}^2 - \frac{1}{3}\omega^3\right)\left[\frac{\tilde{\omega}_{na} + \omega + \frac{i}{2}\Gamma_{na}}{(\tilde{\omega}_{na}+\omega)^2 + \frac{1}{4}\Gamma_{na}^2} + \frac{\tilde{\omega}_{na} - \omega + \frac{i}{2}\Gamma_{na}}{(\tilde{\omega}_{na}-\omega)^2 + \frac{1}{4}\Gamma_{na}^2}\right], \quad (47)$$

where we used the relation $(\vec{p})_{ab} = i\omega_{ab}(\vec{r})_{ab}$ and the notation $\tilde{\omega}_{na} = E_n - E_a + \Delta E_{na}^L$. Then, the real part is defined by

$$\mathrm{Re}\widetilde{\Delta E}_a^{\beta} = -\frac{e^2}{\pi}\sum_n |\langle a|\vec{r}|n\rangle|^2 \int_0^{\infty} d\omega\, n_\beta(\omega)\left(\omega\tilde{\omega}_{an}^2 - \frac{1}{3}\omega^3\right)\left[\frac{\tilde{\omega}_{na} + \omega}{(\tilde{\omega}_{na}+\omega)^2 + \frac{1}{4}\Gamma_{na}^2} + \frac{\tilde{\omega}_{na} - \omega}{(\tilde{\omega}_{na}-\omega)^2 + \frac{1}{4}\Gamma_{na}^2}\right]. \quad (48)$$

The level width Γ_{na} in energy denominators of Eq. (48) becomes important within the resonance only for the values $\omega = \tilde{\omega}_{na} < 0$ or $\omega = \tilde{\omega}_{na} > 0$. The ac Stark shift is considered usually in off-resonance case when the bulk of the BBR distribution lies far from the atomic transitions. Then, the width Γ_{na} in denominators of Eq. (48) can be omitted since $\Gamma_{na} \ll \Delta E_{na}^L$. Thus, a similar result of Eq. (32) again arises which only differs by the replacement $\omega_{an} \to \tilde{\omega}_{an}$:

$$\mathrm{Re}\widetilde{\Delta E}_a^{\beta} = -\frac{2e^2}{\pi}\sum_n |\langle a|\vec{r}|n\rangle|^2 \int_0^{\infty} d\omega\, n_\beta(\omega)\left[\omega\tilde{\omega}_{an}^2 - \frac{1}{3}\omega^3\right]\frac{\tilde{\omega}_{na}}{\tilde{\omega}_{na}^2 - \omega^2} \approx -\frac{4e^2}{3\pi}\sum_n |\langle a|\vec{r}|n\rangle|^2 \int_0^{\infty} d\omega\, n_\beta(\omega)\omega^3 \frac{\tilde{\omega}_{na}}{\tilde{\omega}_{na}^2 - \omega^2}. \quad (49)$$

Substitution of the dimensionless variable $x = \beta\omega$ yields

$$\mathrm{Re}\widetilde{\Delta E}_a^{\beta} = -\frac{4e^2}{3\beta^2\pi}\sum_n |\langle a|\vec{r}|n\rangle|^2 \int_0^{\infty} dx \frac{x^3}{e^x - 1}\frac{\tilde{\omega}_{na}}{\beta^2\tilde{\omega}_{na}^2 - x^2}. \quad (50)$$

Formally, this expression coincides with Eq. (32) with the only difference that the ordinary Lamb shift is included explicitly in $\tilde{\omega}_{na}$.

We should note that the complete BBR-induced energy shift ordinary is given by the real part of Eq. (45) where no approximations were used. In the nonrelativistic limit, we obtain the result (50) which can be evaluated further for the limiting cases of low or high temperatures (see Refs. [18–20] for details). In the low-temperature regime, the bulk of $n_\beta(\omega)$ lies in the region where $x \ll \beta\omega_{na}$ (the off-resonance case) and, therefore, in Eq. (50) the leading term is

$$\mathrm{Re}\widetilde{\Delta E}_a^{\beta} = -\frac{4e^2}{3\beta^4\pi}\sum_n \frac{|\langle a|\vec{r}|n\rangle|^2}{\tilde{\omega}_{na}} \int_0^{\infty} dx \frac{x^3}{e^x - 1}. \quad (51)$$

Integration over x leads to

$$\mathrm{Re}\widetilde{\Delta E}_a^{\beta} = -\frac{4e^2\pi^3}{45\beta^4}\sum_{n\neq a}\frac{|\langle a|\vec{r}|n\rangle|^2}{\tilde{\omega}_{na}}\ \text{r.u.} = -\frac{1}{3}\langle E^2\rangle_t \sum_{n\neq a}\frac{|\langle a|\vec{r}|n\rangle|^2}{E_n - E_a}\ \text{a.u.}, \quad (52)$$

where we used definition (4).

Expression (52) represents the *static* Stark shift. The result (52) was obtained in the low-temperature regime and is proportional to the fourth degree of temperature. In this case, the influence of the photon distribution can be considered as the external field

with the electric field strength corresponding to rms value (4). In principle, the low-temperature regime ($x \ll \beta\tilde{\omega_{na}}$) is applicable for nondegenerated states only. In case of degenerated (Lamb shifted) states, the high-temperature regime should be employed. In this case, the Stark shift is proportional to β^2 [20] (see also [2]). For example, the presence of $n = 2p$ state in the sum in Eq. (52) for $a = 2s$ makes the condition $x \ll \beta\tilde{\omega}_{na}$ much more restrictive since $\tilde{\omega}_{2p\,2s}$ is relatively small. Then, the low-temperature regime for $a = 2s$, $n = 2p$ term in hydrogen starts for much lower temperatures than for $a = 2s$, $n \neq 2p$.

B. Mixing effect and BBR-Stark-induced level width

The results obtained in the previous subsection are in perfect agreement with [18–20]. Furthermore, the QED regularization leads to the appearance of the imaginary part in energy denominators that is responsible for the additional effect of the BBR mixing of states. It is well known that the external electric field leads to the Stark mixing of states. This effect is most pronounced for close-lying states ($2s_{1/2}$ and $2p_{1/2}$ states in hydrogen, for example). As it was shown in [21–24], the influence of an external electric field on the $2s$ state in hydrogen atom can be described by the modified wave function

$$\left|\overline{2s}m_{j_s}\right\rangle = \left|2sm_{j_s}\right\rangle + \eta\sum_{m_{jp}}\left\langle 2pm_{j_p}\left|e\mathbf{Dr}\right|2sm_{j_s}\right\rangle\left|2pm_{j_p}\right\rangle, \quad \eta = \frac{1}{\Delta E_L + i\Gamma_{2p}/2}, \tag{53}$$

where $m_{j_{s(p)}}$ corresponds to the projection of the total angular momentum $j_{s(p)}$ of the $s(p)$ state on the field direction, ΔE_L is the Lamb shift, Γ_{2p} is the level width of the $2p$ state. The matrix element $\langle 2pm_{j_p}|e\mathbf{Dr}|2sm_{j_s}\rangle$ represents the dipole interaction of the atomic electron with the external electric field $\mathbf{D}$.

Then, the one-photon emission amplitude is

$$U_{\overline{2s}m_{j_s},\,1sm'_{j_s}}(\mathbf{k},\mathbf{e}) = U_{2sm_{j_s},\,1sm'_{j_s}}(\mathbf{k},\mathbf{e}) + \eta\sum_{m_{jp}}\left\langle 2s\,m_{j_s}\left|e\mathbf{Dr}\right|2p\,m_{j_p}\right\rangle U_{2pm_{jp},\,1sm'_{j_s}}(\mathbf{k},\mathbf{e}), \tag{54}$$

where $\mathbf{k}$ is the photon wave vector and $\mathbf{e}$ is the photon polarization vector. Within a QM approach, the one-photon decay rate of the mixed $\overline{2s}$ state can be presented in the form [21–24] (in r.u.)

$$dW^{(1\gamma)}_{\overline{2s},\,1s}(\mathbf{n_k}) = dW^{(1\gamma)}_{2s\,1s}(\mathbf{n_k})\left[1 + ea_0\mathbf{Dn_k}|\eta|^2\frac{\Gamma_{2p}}{w^{(1\gamma)}} + |\eta|^2\frac{e^2a_0^2\mathbf{D}^2}{(w^{(1\gamma)})^2}\right]d\mathbf{n_k}. \tag{55}$$

Here, $\mathbf{n_k}$ is the unit vector of the photon emission direction, $w^{(1\gamma)} = \sqrt{W^{(1\gamma)}_{2s,\,1s}/W^{(1\gamma)}_{2p,\,1s}}$, and a_0 is the Bohr radius. The one-photon transition probabilities $W^{(1\gamma)}_{2s,\,1s}$ and $W^{(1\gamma)}_{2p,\,1s}$ correspond to the emission of the magnetic dipole and electric dipole photons, respectively. Integration over photon emission direction leads to the expression

$$W^{(1\gamma)}_{\overline{2s},\,1s} = W^{(1\gamma)}_{2s\,1s} + \frac{e^2a_0^2D^2}{\Delta E_L^2 + \frac{1}{4}\Gamma_{2p}^2}W^{(1\gamma)}_{2p,\,1s}. \tag{56}$$

This expression shows that the additional one-photon electric dipole emission channel is allowed for the atom in metastable $2s$ state in presence of an external electric field. Since the decay rate of $E1$ transition $W^{(1\gamma)}_{2p,\,1s} = 6.265\times10^8\ \mathrm{s}^{-1}$ exceeds strongly not only the one-photon magnetic decay rate $W^{(1\gamma)}_{2s,\,1s} = 2.495\,76\times10^{-6}\ \mathrm{s}^{-1}$, but also the main decay channel of $2s$ state in the absence of electric field $W^{(2\gamma)}_{2s,\,1s} = 8.229\ \mathrm{s}^{-1}$, the second term in Eq. (56) may become the dominant decay channel of $\overline{2s}$ state for moderate external electric fields. The complete mixing of the $2s$ and $2p$ states in hydrogen corresponds to the field 475 V/cm. In that case, the decay of the $\overline{2s}$ state occurs with the emission of the electric dipole photon and corresponding transition rate is equal to the decay rate of the $2p$ state. Hence, the rms value (4) could lead to the effect of mixing in the blackbody radiation of the order of 10^{-3}–10^{-4} times less than the full mixing field 475 V/cm at the temperature 300 K.

The term linear in the field in Eq. (55) vanishes after the integration over photon emission directions or after the integration over field directions. In contrast, the term quadratic in the field does not depend on the photon emission or field directions. Therefore, it should be present in any isotropic external fields (blackbody radiation, for example). To describe the *quadratic mixing* of states in presence of an isotropic field we consider Eq. (45), i.e., take into account the distribution function $n_\beta(\omega)$. Then, the imaginary part of Eq. (47) in the nonrelativistic limit and in the resonance approximation is given by

$$\mathrm{Im}\widetilde{\Delta E}_a^{\beta\,\prime} = -\frac{e^2}{3\pi}\sum_n|\langle a|\vec{r}|n\rangle|^2\int_0^\infty d\omega\, n_\beta(\omega)\omega^3\left[\frac{\Gamma_{na}}{(\tilde{\omega}_{na}+\omega)^2+\frac{1}{4}\Gamma_{na}^2} + \frac{\Gamma_{na}}{(\tilde{\omega}_{na}-\omega)^2+\frac{1}{4}\Gamma_{na}^2}\right]. \tag{57}$$

The "prime" symbol in the left-hand side of Eq. (57) indicates that now we consider another imaginary contribution to $\widetilde{\Delta E}_a^{\beta}$, different from the contribution (36). This imaginary contribution describes a different physical effect: Eq. (36) corresponds to the level depopulation by the BBR while Eq. (57) describes the additional broadening due to the Stark level mixing.

The leading term in low-temperature approximation [see Eqs. (51) and (52)] is

$$\mathrm{Im}\widetilde{\Delta E}_a^{\beta\prime} \approx -\frac{2e^2}{3\pi}\sum_n |\langle a|\vec{r}|n\rangle|^2 \int_0^\infty d\omega\, n_\beta(\omega)\omega^3 \frac{\Gamma_{na}}{\tilde{\omega}_{na}^2 + \frac{1}{4}\Gamma_{na}^2}. \tag{58}$$

Then, for the additional BBR width Γ_a^{mix} induced by the mixing effect we obtain

$$\Gamma_a^{\mathrm{mix}} = \frac{4e^2}{3\pi}\sum_n \frac{|\langle a|\vec{r}|n\rangle|^2}{\tilde{\omega}_{na}^2 + \frac{1}{4}\Gamma_{na}^2}\Gamma_{na}\int_0^\infty d\omega\, n_\beta(\omega)\omega^3 = \frac{4e^2\pi^3}{45}(kT)^4\sum_n \frac{|\langle a|\vec{r}|n\rangle|^2}{\tilde{\omega}_{na}^2 + \frac{1}{4}\Gamma_{na}^2}\Gamma_{na}\ \text{r.u.} = \frac{1}{3}\langle E^2\rangle_t \sum_n \frac{|\langle a|\vec{r}|n\rangle|^2}{\tilde{\omega}_{na}^2 + \frac{1}{4}\Gamma_{na}^2}\Gamma_{na}\ \text{a.u.} \tag{59}$$

In particular, for hydrogen atom for very low temperature the leading term in the sum in Eq. (59) will be given by mixing of $2s_{1/2}$ and $2p_{1/2}$ states.

In the high-temperature regime, we should use condition $\Gamma_{na} \ll \tilde{\omega}_{na} \ll \omega$. At any values of n we find

$$\Gamma_a^{\mathrm{mix}} = \frac{4e^2}{3\pi}\sum_n |\langle a|\vec{r}|n\rangle|^2\Gamma_{na}\int_0^\infty d\omega\, n_\beta(\omega)\omega = \frac{2e^2\pi}{9}(kT)^2\sum_n |\langle a|\vec{r}|n\rangle|^2\Gamma_{na}. \tag{60}$$

The expressions (59) and (60) represent the rough estimates and it is more adequate to use

$$\Gamma_a^{\mathrm{mix}} = \frac{2e^2}{3\pi}\sum_n |\langle a|\vec{r}|n\rangle|^2 \int_0^\infty d\omega\, n_\beta(\omega)\omega^3\left[\frac{\Gamma_{na}}{(\tilde{\omega}_{na}+\omega)^2 + \frac{1}{4}\Gamma_{na}^2} + \frac{\Gamma_{na}}{(\tilde{\omega}_{na}-\omega)^2 + \frac{1}{4}\Gamma_{na}^2}\right]. \tag{61}$$

VI. NUMERICAL RESULTS, TECHNICAL DETAILS, AND DISCUSSION

In this section, we present numerical results of our evaluation of the Stark shifts and widths for different states a in the hydrogen atom. The Stark shift and BBR-induced width we compare with the results of [2]. The new object of this paper, the BBR-Stark-induced level width Γ_a^{mix}, is evaluated for different states in hydrogen atom and should be compared with data on the spectroscopic measurements of hydrogen atom.

In Table I, the results of numerical evaluation of ac Stark shift [Eq. (32)] are shown. We recall that Eq. (32) coincides exactly with the result of quantum mechanical derivation in [1,2]. Thus, the deviation between our calculations and numbers given in [2] should be attributed to the method of numerical evaluation. The summation over discrete set of intermediate states up to $n = 10$ gives a good agreement with the results of Farley and Wing [2]. The following increasing of the set of intermediate states up to $n = 100$ leads to a correction of the order of 0.8% and increasing the set up to $n = 1000$ to correction of the order 1% for the $1s$ and $2s$ states in hydrogen atom. The inclusion of the continuous spectrum gives rise to a contribution of about 19% of the total value at high temperature, but it seems to be negligible for low temperatures. Note also that we can reproduce the values of ac Stark shift for the $1s$ and $2s$ states in hydrogen atom at temperatures $T = 300$, 4, and 77 K reported in [25] with six digits. The deviation from [2] remains the same (in a second digit) for all ns ($n = 1$–5) states.

Inclusion of the ordinary Lamb shift becomes important for the excited states beginning from the $2s$ level. For the $2s$ state, the contribution that comes from $n = 2p$ state is smaller compared to the value of the total sum $-0.989\,702$ (see Table I) and gives $0.007\,001\,39$ Hz at the temperature $T = 300$ K. However, the $n = 2p$ term produces the main contribution at the low temperatures: $7.166\,69 \times 10^{-7}$ Hz at the temperature $T = 3$ K and $2.383\,56 \times 10^{-6}$ at $T = 5.5$ K. The difference between numerical evaluations by Eqs. (32) and (50) is exhibited at low temperatures only when the contribution of the Lamb shift is included. Thus, the regularization of the divergent energy denominators in Eq. (25) does not lead to essential changes of the BBR-induced Stark shift in laboratory experiments at the room BBR temperature but may become important for the lowest temperatures of the order of a few Kelvin. The numerical evaluation was performed utilizing the *Mathematica* code by the trapezoidal method with a working precision of 50 digits.

In [2] it was noted that the ac Stark shift changes its sign with increasing of n. From Table I it follows that BBR-induced energy shift also changes its sign with increasing of the temperature. For the $2s$ and $3s$ states, this temperature is about 25–30 K and 10–15 K, respectively.

For the $4s$ state in hydrogen atom the ac Stark shift turns to zero at the two points: at low temperature: about 10 K and at high temperatures about 4000–5000 K. The behavior of the ac Stark shift for the $5s$ state repeats the case of $4s$ state: at the low temperature about 5 K the energy shift is equal to zero and at the high temperature 607 K it also turns to zero. In principle, such behavior provides the method to avoid the Stark shift induced by the blackbody radiation. The ac Stark shift evaluated with Eq. (32) and depending on the temperature is shown in Figs. 3 and 4. In Fig. 3, the behavior of the ac Stark shift for the $5s$ state in hydrogen atom for the temperature region [100, 650] K and in Fig. 4 the same for temperature region [0, 3.5] K is depicted. In Fig. 3, the contribution of the Lamb shift is multiplied by the factor 10^3 to make it visible. The total contribution of the discrete, Lamb shifted, and continuum states to the energy shift of the state $5s$ in hydrogen atom is depicted in Fig. 5 for the temperature region [200, 700] K.

In Table II, the results of numerical evaluation of Eq. (37) are compiled, i.e., the BBR-induced level widths for the different states a and different temperatures T. As before,

TABLE I. The ac Stark shift induced by the blackbody radiation in Hz for the ns states in the hydrogen atom for different temperatures T. The first column contains the considered n values. In the second column, the lower line for each n value presents the results of [2]. The asterisk corresponds to the values evaluated without inclusion of continuous spectrum.

a	$T = 300$ K	$T = 3$ K $*$	$T = 5.5$ K $*$	$T = 3000$ K	$T = 4000$ K	$T = 5000$ K
$1s$	$-0.038\,7511$	-3.1542×10^{-10}	$-3.563\,32 \times 10^{-9}$	-391.455	-1247.01	-3079.38
	$-0.041\,28$					
$2s$	$-0.989\,702$	$7.071\,28 \times 10^{-7}$	$2.275\,78 \times 10^{-6}$	$-22\,348.9$	$-95\,953.1$	$-2.525\,46 \times 10^{5}$
	-1.077					
$3s$	$-8.939\,74$	$1.280\,21 \times 10^{-6}$	$3.643\,41 \times 10^{-6}$	$-2.767\,04 \times 10^{5}$	$-5.729\,30 \times 10^{5}$	$-8.880\,17 \times 10^{5}$
	-9.103					
$4s$	-50.1879	$1.338\,48 \times 10^{-6}$	$1.150\,04 \times 10^{-6}$	$-5.837\,84 \times 10^{4}$	$-5.794\,27 \times 10^{4}$	8.4836×10^{3}
	-51.19					
$5s$	-186.884	$6.242\,76 \times 10^{-7}$	$-9.941\,88 \times 10^{-6}$	$1.931\,86 \times 10^{5}$	$3.800\,32 \times 10^{5}$	$6.196\,69 \times 10^{5}$
	-209.5					

the values of Γ_a^β should be compared with the results of [2] at the temperature 300 K for the hydrogen atom. The level widths Γ_a^β are important not only in laboratory experiments, but in astrophysical investigations of the cosmic microwave background (see [26] and references therein). For the further analysis, we evaluate the widths Γ_a^β at high temperatures which we associated with the temperatures of the universe in the recombination epoch. Note that the value of Γ_{2s}^β at the temperature 3000 K coincides with the value reported in [25] but differs from [25] at the temperature 300 K though our result coincides with the result of [2].

The numbers in Table II should be compared with the natural level widths. The most precise value of the Γ_{2s} was obtained in [27]. The radiative correction of the leading order in αZ expansion leads to the contribution -2.057×10^{-6} s^{-1} [27] which is even less than BBR-induced depopulation rate at the temperature 300 K (see first column in Table II). Thus, we can conclude that the influence of blackbody radiation is more significant and screens the radiative corrections to the level width in experiments. Moreover, the increasing of temperature leads to more significant contribution of the BBR-induced level width according to Eq. (37). At temperatures of a few thousands Kelvin (ionization temperatures), the BBR-induced depopulation rate can be comparable and can exceed the natural linewidth. Similar to the case of Stark shift evaluation, the dominant contribution at low temperatures arises due to the Lamb shift between $ns_{1/2}$ and $np_{1/2}$ states. The Lamb shift contribution decreases with the increase of the temperature and becomes unimportant at temperatures $T > 300$ K. With the growing of the principal quantum number of the state a, such behavior is more pronounced.

In Table III, the results of numerical evaluation for $\Gamma_a^{\rm mix}$ according to Eq. (61) for the different states a and temperatures T are presented. The widths $\Gamma_a^{\rm mix}$ we associate with the effect of mixing of atomic states in presence of an external field [21–24]. The values of level widths are given in Hz. The result for the $2s$ state at the temperature 300 K can be compared with the data indicated for the laboratory experiments with hydrogen atom [28,29] (see also [30]). The contributions of Γ_a^β and $\Gamma_a^{\rm mix}$ become larger than the natural level width at high temperatures.

At low temperatures, the main contribution to the level width $\Gamma_a^{\rm mix}$ arises via the Lamb shifted (degenerated atomic levels) states. This contribution grows quadratically with the increasing temperature. Summation over other intermediate states leads to the correction about four orders smaller. This is true up to the temperature $\sim$1000 K when the opposite behavior

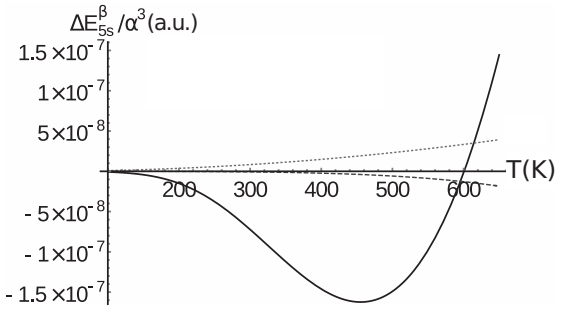

FIG. 3. The temperature dependence of the ac Stark shift for the $5s$ state in hydrogen atom in the region [100, 650] K. On the horizontal axis, the temperature in K and on the vertical axis the ac Stark shift in atomic units divided by α^3 are plotted. The solid line corresponds to the summation over discrete spectrum, dashed line denotes the contribution of the continuum. The Lamb shift contribution is multiplied by the factor 10^3 and depicted by the dotted line.

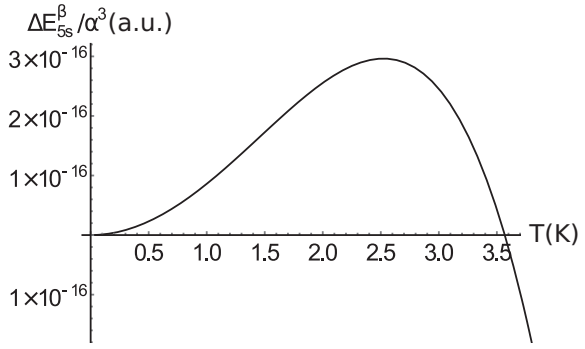

FIG. 4. The temperature dependence of the total contribution of ac Stark shift for the $5s$ state in hydrogen atom in the region [0, 3.5] K. On the horizontal axis, the temperature in K and on the vertical axis the ac Stark shift in atomic units divided by α^3 are plotted.

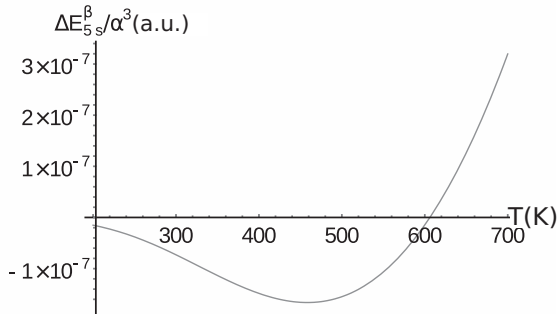

FIG. 5. The temperature dependence of the ac Stark shift for the $5s$ state in hydrogen atom in the region [200, 700] K. Notations are the same as in Figs. 3 and 4.

can be noted. At high temperatures, the main contribution arises from the summation over the full set of intermediate states which leads to the growth of the width proportional to the $(kT)^4$. The contribution of the continuum spectrum is negligible at low temperatures and becomes important for higher-lying states and higher temperatures. To evaluate the values listed in Table III, we performed the summation over intermediate states up to $n = 10$ for the $2s$ state. The additional summation over n leads to the correction five orders smaller than the main contribution.

The quadratic level mixing effect can be important also in astrophysics, for description of the radiation escape from the matter in the early universe in cosmological recombination epoch. The modern theory of the cosmological recombination starts with works by Zel'dovich, Kurt, and Sunyaev [31] and Peebles [32] where it was found that the two-photon $2s \to 1s + 2\gamma(E1)$ transition is one of the main channels for the radiation escape and formation of the cosmic microwave background (CMB). This conclusion is based on the smallness of the one-photon transition $2s \to 1s + 1\gamma(M1)$: $W^{M1}_{2s\text{-}1s} = 2.8 \times 10^{-6}$ s^{-1}. It is well known that the radiation properties of CMB can be described as BBR. Then, using the results in Table III for $\Gamma^{\rm mix}_a$ at $T = 3000$ K (the CMB temperature at the epoch of cosmological recombination) we find $\Gamma^{\rm mix}_a(T = 3000\ {\rm K}) = 7.4 \times 10^8$ Hz, which is 14 orders of magnitude larger than $W^{M1}_{2s\text{-}1s}$ and is of the same order of magnitude as the Lyman-alpha transition probability $W^{E1}_{2p\text{-}1s}$. This may have serious consequences for the primordial hydrogen recombination theory.

VII. CONCLUSIONS

In this paper, we reexamined the influence of the blackbody radiation on the atom. The rigorous derivation of the Stark shift and BBR-induced level width was presented within the framework of quantum electrodynamics. For this purpose, the photon propagator (24) derived within the finite-temperature QED in [12] was used. This propagator includes the distribution function of photon number $n_\beta(\omega)$. Moreover, the propagator (24) allows for the description of the BBR influence on an atom with the standard technique corresponding to the self-energy correction for the bound electron. As in the ordinary case, the real part of such one-loop correction represents the Stark shift and imaginary part corresponds to the BBR-induced level width. The depopulation rate Γ^β_a [Eq. (37)] and Stark shift [Eq. (32)] are in the exact agreement with the results of quantum mechanical derivation [2].

The QED approach demonstrates clearly the existence of another important contribution to the level broadening via the quadratic mixing of the levels with opposite parity by the BBR mean electric field. This contribution $\Gamma^{\rm mix}_a$ can be described phenomenologically also within the QM approach, however, the QED derivation reveals most clearly that this effect is distinct from the well-known BBR level broadening effect due to the atomic level depopulation. The mixing of atomic states by the stray electric field was considered in [21] as an effect which can mimic the parity violation effect. However, in [21] the linear in the electric field effect was described. We consider the effect of level mixing quadratic in the electric field, which can arise due to the mean BBR electric field. We should mention also that the QED theory for the atom in the heat bath can be reformulated in terms of the "thermal excitation potential" introduced earlier by Low [33].

To check the numerical evaluation of $\Gamma^{\rm mix}_a$ we have calculated the Stark shift and depopulation rates Γ^β_a for the different states and temperatures. The results of numerical calculations are presented in Tables I and II and Figs. 3–5 and are in good agreement with the results reported in [2,25]. The dependence on temperatures revealed also that the the Stark shift can tend to zero at certain temperatures. This behavior corresponds to the Stark shift quadratic in the field only: the Stark shift linear in the mean BBR electric field is absent due to the absence of a preferred direction and the Stark shift arising due to the next orders in the field gives the small corrections. There are two values for the temperature where

TABLE II. The BBR-induced depopulation rates in s^{-1} for the ns states in hydrogen atom Eq. (37) for the different temperatures T. The first column contains the considered n values. In the second column, the lower line for each n value presents the results of [2]. The asterisk corresponds to the values evaluated without inclusion of continuum spectrum. In the last column, the natural level widths in s^{-1} are given.

a	$T = 300$ K	$T = 3$ K $*$	$T = 5.5$ K $*$	$T = 3000$ K	$T = 4000$ K	$T = 5000$ K	Γ_a
$2s$	$1.422\,81\times10^{-5}$ 1.42×10^{-5}	$1.434\,77\times10^{-7}$	$2.620\,32\times10^{-7}$	$4.703\,76\times10^{4}$	$3.072\,69\times10^{5}$	$9.773\,95\times10^{5}$	8.229 352 436
$3s$	$8.035\,35\times10^{-5}$ 7.97×10^{-5}	9.0978×10^{-8}	$1.665\,84\times10^{-7}$	$9.893\,31\times10^{5}$	$2.281\,31\times10^{6}$	$4.031\,77\times10^{6}$	$6.316\,96\times10^{6}$
$4s$	15.9454 16.02	4.5077×10^{-8}	$8.260\,11\times10^{-8}$	$1.756\,29\times10^{6}$	$3.184\,43\times10^{6}$	4.861×10^{6}	$4.415\,94\times10^{6}$
$5s$	1196.44 1199	2.6374×10^{-8}	4.8341×10^{-8}	$1.933\,56\times10^{6}$	$3.160\,22\times10^{6}$	$4.526\,55\times10^{6}$	$2.839\,91\times10^{6}$

TABLE III. The Stark-mixing level widths Eq. (61) in Hz (s^{-1} divided by 2π) for the ns states in hydrogen atom are listed for the different temperatures T. The first column contains considered n values. The second subline in each row gives the values of $\Gamma_a^{\rm mix}$ in Hz without the account for Lamb shift.

a	$T = 300$ K	$T = 270$ K	$T = 77$ K	$T = 3$ K $*$	$T = 5.5$ K $*$	$T = 3000$ K	$T = 4000$ K	Γ_a
$2s$	$1.703\,23\times10^3$	$1.380\,12\times10^3$	113.303	0.227 06	0.676 15	$7.402\,97\times10^8$	4.6187×10^9	1.309 74
	0.140 134	0.091 7596	$6.022\,85\times10^{-4}$	1.3868×10^{-9}	1.5667×10^{-8}	$7.401\,28\times10^8$	4.6184×10^9	
$3s$	$3.191\,83\times10^3$	2.5854×10^3	210.861	0.355 491	1.138 65	$2.561\,46\times10^8$	$1.496\,32\times10^9$	$1.005\,38\times10^6$
	1.875 93	1.207 8	$7.487\,49\times10^{-3}$	1.7143×10^{-8}	$1.936\,69\times10^{-7}$	$2.558\,28\times10^8$	$1.495\,75\times10^9$	
$4s$	$5.272\,02\times10^3$	$3.968\,44\times10^3$	310.502	0.489 158	1.6157	$4.452\,45\times10^8$	$1.047\,48\times10^9$	$7.028\,19\times10^5$
	627.656	206.34	4.190 82	$6.574\,23\times10^{-3}$	0.021 6627	$4.447\,81\times10^8$	$1.046\,66\times10^9$	
$5s$	$3.993\,57\times10^4$	$2.131\,01\times10^4$	400.95	0.618 677	2.062 95	$5.549\,16\times10^7$	$8.566\,09\times10^7$	$4.519\,86\times10^5$
	$3.385\,59\times10^4$	$1.638\,54\times10^4$	0.218 588	4.612×10^{-7}	$5.211\,71\times10^{-6}$	$5.488\,37\times10^7$	$8.458\,02\times10^7$	

the Stark shift [Eq. (32)] vanishes. The first one corresponds to the low temperature and another to the high temperature. For the higher excited state, the upper zeroth point is achieved at lower temperature. So, for the $4s$ state the point where quadratic Stark shift is equal to zero lies between 4000 and 5000 K although for the $5s$ state this point was found close to 600 K.

The results of evaluation of $\Gamma_a^{\rm mix}$ at high temperatures show that this effect can be important in astrophysical study of the cosmic microwave background where the $2s$ state plays the crucial role in recombination processes for the primordial hydrogen atoms. More detailed investigations on the subject will be presented elsewhere as separate publication.

ACKNOWLEDGMENTS

This work was supported by RFBR (Grant No. 14-02-00188). D.S. and L.L. acknowledge the support by St.-Petersburg State University with a research Grant No.11.38.227.2014. D.S. also acknowledges financial support by the Max-Planck Institut für Physik komplexer Systeme and for kind hospitality by the Dresden University of Technology.

[1] T. F. Gallagher and W. E. Cooke, Phys. Rev. Lett. **42**, 835 (1979).
[2] J. W. Farley and W. H. Wing, Phys. Rev. A **23**, 2397 (1981).
[3] M. S. Safronova, Dansha Jiang, Bindiya Arora, Charles W. Clark, M. G. Kozlov, U. I. Safronova, and W. R. Johnson, IEEE Trans. Ultrason. Ferroelectrics Freq. Control **57**, 94 (2010).
[4] S. G. Porsev and A. Derevianko, Phys. Rev. A **74**, 020502(R) (2006).
[5] C. Degenhardt *et al.*, Phys. Rev. A **72**, 062111 (2005).
[6] M. S. Safronova, M. G. Kozlov, and Charles W. Clark, Phys. Rev. Lett. **107**, 143006 (2011).
[7] Wayne M. Itano, L. L. Lewis, and D. J. Wineland, Phys. Rev. A **25**, 1233 (1982).
[8] Th. Middelmann, Ch. Lisdat, St. Falke, J. S. R. Vellore Winfred, F. Riehle and U. Sterr, IEEE Trans. Instrum. Meas. **60**, 2550 (2011).
[9] J.-L. Robyr, P. Knowles, and A. Weis, in *IEEE International Joint Conference on Frequency Control and the European Frequency and Time Forum (FCS), 2011* (IEEE, Piscataway, NJ, 2011), pp. 1–4.
[10] E. N. Forston, D. Kleppner, and N. F. Ramsey, Phys. Rev. Lett. **13**, 22 (1964).
[11] I. L. Glukhov, E. A. Nekipelov, and V. D. Ovsiannikov, J. Phys. B: At., Mol. Opt. Phys. **43**, 125002 (2010).
[12] J. F. Donoghue and B. R. Holstein, Phys. Rev. D **28**, 340 (1983).
[13] L. Labzowsky, G. Klimchitskaya, and Yu. Dmitriev, *Relativistic Effects in the Spectra of Atomic Systems* (Institute of Physics Publishing, Bristol and Philadelphia, 1993).
[14] O. Yu. Andreev, L. N. Labzowsky, G. Plunien, and D. A. Solovyev, Phys. Rep. **455**, 135 (2008).
[15] T. Zalialiutdinov, D. Solovyev, L. Labzowsky, and G. Plunien, Phys. Rev. A **89**, 052502 (2014).
[16] S. Saleem, Phys. Rev. D **36**, 2602 (1987).
[17] L. N. Labzowsky, A. V. Shonin, and D. A. Solovyev, J. Phys. B: At., Mol. Opt. Phys. **38**, 265 (2005).
[18] J. E. Walsh, Phys. Rev. Lett. **27**, 208 (1971).
[19] G. Barton, Phys. Rev. A **5**, 468 (1972).
[20] P. L. Knight, J. Phys. A: Gen. Phys. **5**, 417 (1972).
[21] Ya. I. Azimov, A. A. Ansel'm, A. N. Moskalev and R. M. Ryndin, Zh. Eksp. Teor. Fiz. **67**, 17 (1974) [Sov. Phys.–JETP **40**, 8 (1975)].
[22] P. J. Mohr, Phys. Rev. Lett. **40**, 854 (1978).
[23] D. A. Solov'ev, V. F. Sharipov, L. N. Labzovskii, and G. Plunien, Opt. Spectrosc. **104**, 509 (2008).
[24] D. Solovyev, V. Sharipov, L. Labzowsky, and G. Plunien, J. Phys. B: At., Mol. Opt. Phys. **43**, 074005 (2010).
[25] U. D. Jentschura and M. Haas, Phys. Rev. A **78**, 042504 (2008).
[26] E. E. Kholupenko and A. V. Ivanchik, Astron. Lett. **32**, 795 (2006).
[27] U. D. Jentschura, Phys. Rev. A **69**, 052118 (2004).
[28] A. Matveev *et al.*, Phys. Rev. Lett. **110**, 230801 (2013).
[29] J. Alnis, A. Matveev, N. Kolachevsky, T. Udem, and T. W. Hansch, Phys. Rev. A **77**, 053809 (2008).
[30] N. Kolachevsky, M. Haas, U. D. Jentschura, M. Herrmann, P. Fendel, M. Fischer, R. Holzwarth, T. Udem, C. H. Keitel, and T. W. Hansch, Phys. Rev. A **74**, 052504 (2006).
[31] Ya. B. Zel'dovich, V. G. Kurt, and R. A. Sunyaev, Zh. Eksp. Teor. Fiz. **55**, 278 (1968) [Sov. Phys.–JETP **28**, 146 (1969)].
[32] P. J. E. Peebles, Astrophys. J. **153**, 1 (1968).
[33] F. Low, Phys. Rev. **88**, 53 (1952).